

Estimating the Black Hole Spin for the X-Ray Binary MAXI J1727-203 Based on Insight-HXMT

HAIFAN ZHU ¹ AND WEI WANG ^{1,*}

¹*Department of Astronomy, School of Physics and Technology, Wuhan University, Wuhan 430072, China*

ABSTRACT

We constrain the spin of the black hole (BH) candidate MAXI J1727-203 using Insight-HXMT data. Due to limited HXMT observations covering only part of the outburst, NICER data were used to analyze the full outburst's state transitions, we identified two of three HXMT observations in the high soft state and applied the continuum-fitting method to measure the spin. Based on previous estimates and continuum spectral fittings, we explored the parameter space and found that the best-fitting values were $(D, i, M) \approx (6 \text{ kpc}, 30^\circ, 12M_\odot)$. We also tested the variation of these parameters using Monte Carlo simulations, sampling over 3000 sets within the parameter ranges: $5.9\text{kpc} < D < 7\text{kpc}$, $24^\circ < i < 35^\circ$, and $10M_\odot < M < 14M_\odot$, yielding a spin measurement of $a = 0.34_{-0.19}^{+0.15}$ (1σ). In addition, we analyzed NuSTAR data in low hard state and found a good fit with the `tbabs*(diskbb+powerlaw)` model, with no significant iron line features observed in the residuals, then the previous reflection model results suggesting an extremely high spin would over-estimate the BH spin.

Keywords: High energy astrophysics (739); Black hole physics (159); Stellar mass black holes (1611); Stellar accretion disks (1579); X-ray transient sources (1852); X-ray sources (1822); X-ray binary stars (1811)

1. INTRODUCTION

Black Hole X-ray Binaries (BHXBs) are binary systems in which a black hole accretes matter from a companion star through Roche lobe overflow. These systems spend most of their time in a quiescent state, with occasional outbursts that can last from weeks to months, during which the X-ray intensity increases by several orders of magnitude compared to the quiescent state. During an outburst, the BHXB evolves through various spectral states (Remillard & McClintock 2006; Belloni 2010). The various spectral states of a BHXB can be broadly categorized as the low hard state (LHS), intermediate state (IMS), and high soft state (HSS). Its evolutionary trajectory starts from LHS, progresses through IMS, then to HSS, and finally returns to LHS, forming a "q"-shaped track in the hardness-intensity diagram (HID, Fender & Belloni 2004).

The black hole spin is a fundamental parameter that provides insights into its formation and evolution while influencing a variety of astrophysical phenomena. The spin parameter of accreting stellar-mass black holes is

commonly measured using two established methods: (1) the continuum-fitting method, which analyzes the thermal emission profile of the accretion disk (Zhang et al. 1997), and (2) the reflection-fitting method, which focuses on the red wing of the relativistically broadened and asymmetric Fe K α line (Fabian et al. 1989; Reynolds & Nowak 2003).

Both methods use a dimensionless parameter, a_* , to represent the black hole spin, defined as $a_* \equiv \frac{a}{M} = \frac{cJ}{GM^2}$, where a_* represents the black hole spin, M and J denote the black hole's mass and angular momentum, respectively (Kerr 1963). Both methods are based on the fundamental assumption that the inner edge of the accretion disk extends to the innermost stable circular orbit (ISCO). The key to measuring the spin lies in estimating the radius of the inner disk, r_{in} , defined as $r_{\text{in}} \equiv \frac{cR_{\text{in}}}{GM}$. It is assumed that R_{in} corresponds to the radius of the ISCO, R_{ISCO} . Since $R_{\text{ISCO}}/(GM/c^2)$ maps the spin parameter a_* in a simple and monotonic manner, determining R_{in} (assuming $R_{\text{in}} = R_{\text{ISCO}}$) directly enables the derivation of the black hole spin a_* (Reynolds & Fabian 2008; Noble et al. 2009; Penna et al. 2010; Kulkarni et al. 2011).

In the continuum-fitting method, the inner disk radius, r_{in} , is determined by fitting the X-ray thermal con-

* Email address: wangwei2017@whu.edu.cn

tinuum from the accretion disk to the Novikov-Thorne thin disk model (Novikov et al. 1973). As a non-relativistic approximation, the disk luminosity can be expressed as $L \approx 2\pi D^2 F (\cos i)^{-1} \approx 4\pi R_{\text{ISCO}}^2 T_{\text{eff}}^4$, where F , T_{eff} , D , and i represent the X-ray flux, effective temperature, distance to the source, and disk inclination angle, respectively. This leads to the relationship $R_{\text{ISCO}} \approx F / (2T_{\text{eff}}^4 (\cos i)^{-1} D^2 M^{-2})$. Therefore, three key dynamical parameters—the black hole mass (M), disk inclination (i), and source distance (D)—are essential for accurately estimating the spin. The spin parameter a_* is inversely proportional to R_{ISCO}/M , implying that a larger black hole mass results in a higher spin. Conversely, an increase in either the inclination angle or the source distance increases the value of R_{ISCO}/M , thereby decreasing the estimated spin parameter (Bardeen et al. 1972; Zhao et al. 2021). In addition, uncertainties in the black hole mass M , the source distance D , and the inclination angle i of the accretion disk can also impact the measurement. These factors represent the main sources of systematic uncertainty in the continuum-fitting method.

MAXI J1727-203 was discovered by the MAXI/GSC nova alert system on 2018 June 5 as an uncatalogued X-ray transient located at (RA, Dec) = (261.971°, -20.389°) (J2000) with a 90% confidence elliptical error region of $0.33^\circ \times 0.28^\circ$ (Yoneyama et al. 2018). Ludlam et al. (2018) and Kennea et al. (2018) reported same-day observations of MAXI J1727-203 using the Neutron star Interior Composition Explorer (NICER) and the Neil Gehrels Swift Observatory, respectively. Energy spectral softening observed by MAXI/GSC, combined with the detection of an ultra-soft component with a low disk temperature and large inner disk radius, strongly suggests that MAXI J1727-203 is a black hole binary (Negoro et al. 2018). Then a soft to hard transition was observed with Swift/XRT (Tomsick et al. 2018).

Alabarta et al. (2020) presented an X-ray study of MAXI J1727-203’s 2018 outburst using NICER data. The source exhibited soft and hard spectral components, evolving through HSS, IMS, and LHS. The disk component was detected throughout the outburst, with temperatures dropping from ~ 0.4 keV to ~ 0.1 keV. The power spectrum showed broad-band noise up to 20 Hz, with no QPOs. The fractional rms increased with energy, except in the hard state, where it remained constant. The spectral and timing evolution suggest the system hosts a black hole. Wang et al. (2022) also studied the X-ray spectral and timing evolution of MAXI J1727 - 203 using NICER and MAXI/GSC data, and observed a transition from the IMS to the HSS, and

back to the LHS. In the HSS, the innermost radius remained constant. Assuming a Schwarzschild black hole, the mass was estimated to be $M \geq 11.5M_\odot$ and $D \geq 5.9$ kpc, based on the multi-colour disk model using X-ray, optical and near-infrared multi-wavelength data (Wang et al. 2022).

With the observations from Insight-HXMT and NICER, we try to constrain the spin of the black hole in MAXI J1727-203 using the continuum-fitting method. Section 2 describes the observations and data reduction methods. Section 3 provides the fitting results. Sections 4 and 5 present the discussions and conclusions, respectively.

2. OBSERVATIONS AND DATA REDUCTION

2.1. *Insight-HXMT*

Insight-HXMT is equipped with three distinct types of detectors, each designed for specific energy ranges. The High Energy (HE) detectors operate within the range of 20.0 to 250.0 keV (Liu et al. 2020). The Medium Energy (ME) detectors function between 5.0 and 30.0 keV (Cao et al. 2020). Lastly, the Low Energy (LE) detectors cover a range from 1.0 to 15.0 keV (Chen et al. 2020). The effective areas for these detectors are 5100 cm², 952 cm², and 384 cm², respectively.

The Insight-HXMT observed MAXI J1727-203 three times, and we listed the parameters of each observation in Table 1. Data extraction and analysis were carried out using Version 2.06 of the *Insight-HXMT Data Analysis Software* (HXMTDAS)¹. We processed and filtered the data following the official guidelines, which included maintaining a pointing offset angle of less than 0.04° , ensuring an Earth elevation angle greater than 10° , requiring a geomagnetic cutoff rigidity above 8° , and excluding data collected within 300 seconds of traversing the South Atlantic Anomaly (SAA). Background estimation was performed using HEBKGMAP, MEBKGMAP and LEBKGMAP, while response files were generated through the tasks HERSPGEN, MERSPGEN and LERSPGEN. Due to the higher background count rate in the HE band, we focused our spectral analysis with Insight-HXMT on the energy bands of 1-8.0 keV (LE) and 10-30.0 keV (ME).

2.2. *NICER*

NICER (Gendreau et al. 2016) is an advanced X-ray telescope located on the International Space Station (ISS) that employs silicon-drift detectors, providing a sensitivity range of 0.2 to 12 keV. With an effective area

¹ <http://hxmtcn.ihep.ac.cn/software.jhtml>

Table 1. Information of Insight-HXMT observations on MAXI J1727-203

| ObsID | ExpoID | MJD | Obs data (yyyy-mm-dd) | LE exposure s | ME exposure s | HE exposure s |
|-------------|---------------|-----------|--------------------------|------------------|------------------|------------------|
| P0114758001 | P011475800101 | 58277.229 | 2018-06-08 | 100.747 | 308.206 | 864.204 |
| P0114758001 | P011475800102 | 58277.377 | 2018-06-08 | 1539.141 | 2279.616 | 1109.173 |
| P0114758002 | P011475800201 | 58279.681 | 2018-06-10 | 2692.251 | 2928.097 | 1330.825 |
| P0114758002 | P011475800202 | 58279.846 | 2018-06-10 | 1077.301 | 1033.546 | 1440.614 |
| P0114758003 | P011475800301 | 58282.729 | 2018-06-13 | 2513.701 | 2729.343 | 3137.429 |

exceeding 2000 cm^2 at 1.5 keV and 600 cm^2 at 6 keV, It's time-tagging resolution is less than 300 ns. NICER has a spatial resolution of 5 arcmin in diameter with a non-imaging field of view. The background is primarily dominated by the diffuse cosmic X-ray background in the soft range.

Between June 5 and October 7, 2018, NICER conducted a series of 86 targeted observations of MAXI J1727-203. For our analysis, we utilized the NICER data analysis threads² based on the official HEASOFT V6.32 software, incorporating the calibration files (xti20221001). We employed the tools *nicerl2* and *nicerl3lc* to extract the source and background, respectively. Additionally, we generated light curves using *nicerl3lc* in the energy ranges of 1-4 keV, 4-10 keV, and 1-10 keV.

3. ANALYSIS AND RESULTS

3.1. Light Curves

In the top panel of Figure 1, we presented the background-subtracted light curves for MAXI J1727-203, observed by NICER during the observation period. The variation in the calculated hardness ratio is shown in the bottom panel of Figure 1. All data points have been rebinned to one-day intervals, with IMS, HSS, and LHS represented in red, blue, and yellow, respectively. The time intervals for the different states are as follows: LHS from MJD 58327 to 58397, IMS from MJD 58274 to 58278 and from MJD 58298 to 58327, and HSS from MJD 58278 to 58298. Our classifications are consistent with the results of Alabarta et al. (2020). The positions indicated by the arrows in Figure 1 represent the times of the three observations conducted by Insight-HXMT, while the different colors represent the states of the source during these observations.

We present the hardness-intensity diagram (HID) of MAXI J1727-203 in Figure 2, which provides a clearer view of its evolution throughout the outburst. The

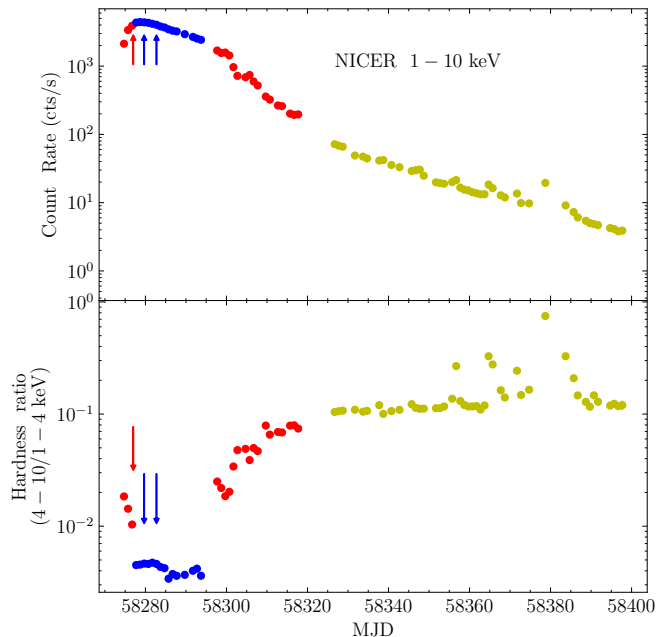


Figure 1. Top panel: NICER 1-10 keV light curve. All data points have been rebinned to one-day intervals, with IMS, HSS, and LHS represented in red, blue, and yellow, respectively. The three arrows indicate the times corresponding to the observations by Insight-HXMT. Bottom panel: Hardness ratios derived from NICER data using (4-10 keV)/(1-4 keV). The arrows and colors have the same meanings as in the top panel. The errors for all data points are at least one order of magnitude smaller than the data points, making them not visible on the plot.

meanings of the colors in the figure are consistent with those in Figure 1. Although we are missing the rise of the outburst, the NICER HID still displays a counter-clockwise Q-shape, signifying transitions from the IMS to the HSS at peak brightness, and from the HSS to the LHS at lower brightness levels.

3.2. The Spectral Analysis

During the three observations by Insight-HXMT, the first observation corresponds to the IMS, while the subsequent two observations correspond to the HSS, with the hardness ratio obtained from NICER data being less

² https://heasarc.gsfc.nasa.gov/docs/nicer/analysis_threads

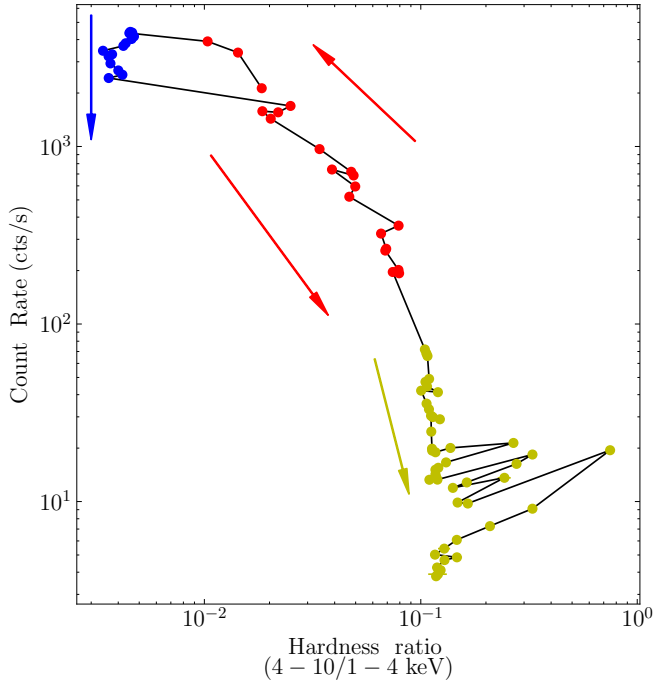


Figure 2. The HID of MAXI J1727-203 during NICER observations. The data points and arrow colors indicate different states, with IMS, HSS, and LHS represented in red, blue, and yellow, respectively. The direction of the arrows indicates the evolution of the outburst process.

than 5×10^{-3} . Therefore, we conducted spectral analysis for these two observations using LE and ME spectral data. We estimated the uncertainties of the parameters using Markov Chain Monte Carlo (MCMC) simulations, employing 8 walkers over a total of 30000 steps. The uncertainties reported in the spectral fitting correspond to the 99 percent confidence level.

3.2.1. Non-Relativistic Model

Firstly, the spectrum is fitted by the multicolour disk blackbody model `diskbb` (Mitsuda et al. 1984; Makishima et al. 1986) and a power-law component: Model 1: `tbabs*(diskbb +powerlaw)`. The `tbabs` model is employed to account for interstellar absorption, using abundances as described by Wilms et al. (2000). This model allows for the adjustment of only the equivalent hydrogen column density, n_H , in units of 10^{22} atoms cm^{-2} . During the fitting process, we set n_H as a free parameter. We present the fitting results in Table 2, examples of the spectra and residuals in Fig 3, and the probability distribution of the parameters in Fig 4. The fitted disk temperature in the first two observations is approximately 0.46 keV, while in the third observation, it decreased to 0.44 keV. Concurrently, the spectral index remained around 2.3 during the first two

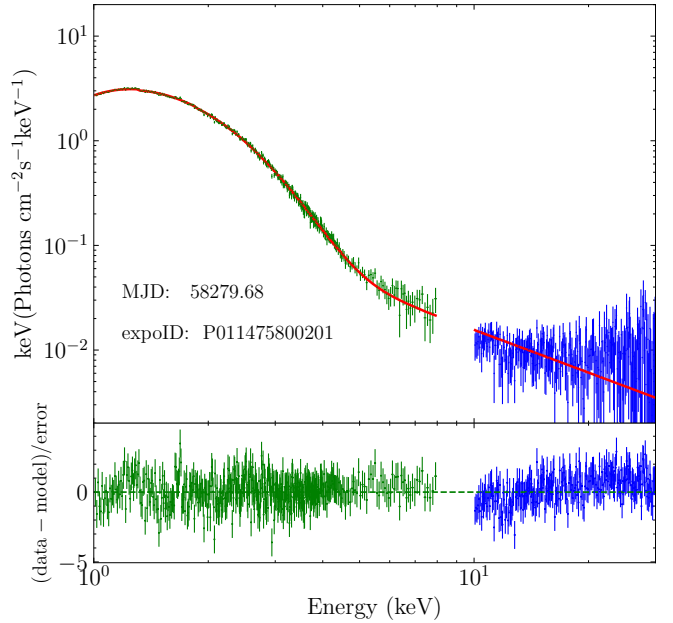


Figure 3. The spectrum and residuals for non-relativistic model are shown as an example. The green and blue data points correspond to LE and ME, respectively. The observation time and expoID are labeled on the plot.

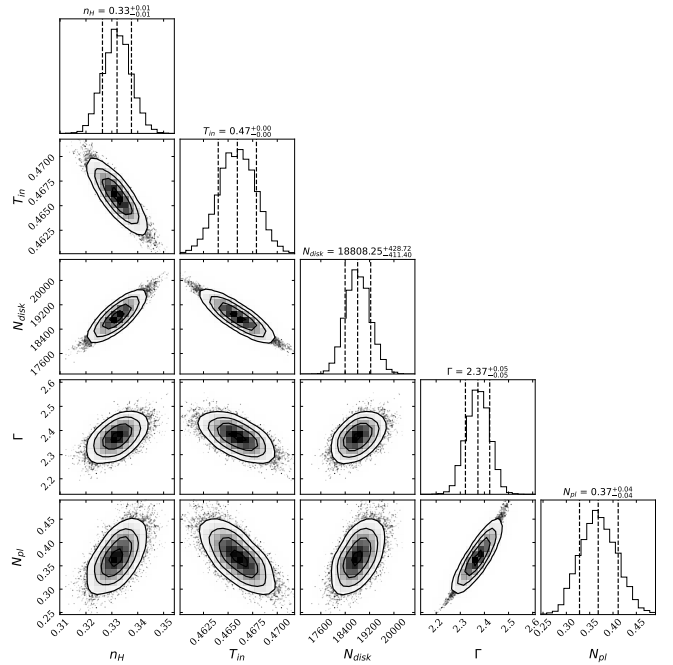


Figure 4. The corner plot of the posterior probability distributions derived from the MCMC analysis for the parameters in the non-relativistic model.

observations but increased to about 2.8 in the third observation.

3.2.2. Relativistic Model

Table 2. The Results of Spectral Fitting the Insight-HXMT Data for Non-Relativistic Model

| Component | Parameter | ExpoID | ExpoID | ExpoID |
|-----------------|--|---------------------------|---------------------------|---------------------------|
| | | P011475800201 | P011475800202 | P011475800301 |
| tbabs | n_{H} [10^{22} cm^{-2}] | $0.33^{+0.02}_{-0.01}$ | $0.33^{+0.02}_{-0.03}$ | $0.39^{+0.02}_{-0.02}$ |
| diskbb | T_{in} [keV] | $0.466^{+0.005}_{-0.006}$ | $0.467^{+0.009}_{-0.007}$ | $0.444^{+0.007}_{-0.008}$ |
| | Norm [10^4] | $1.9^{+0.1}_{-0.1}$ | $1.9^{+0.1}_{-0.2}$ | $2.0^{+0.2}_{-0.1}$ |
| powerlaw | Γ | $2.4^{+0.1}_{-0.1}$ | $2.4^{+0.2}_{-0.1}$ | $2.9^{+0.1}_{-0.1}$ |
| | Norm | $0.4^{+0.1}_{-0.1}$ | $0.4^{+0.2}_{-0.1}$ | $1.4^{+0.3}_{-0.2}$ |
| | χ^2/dof | 0.77 | 0.79 | 0.73 |

After employing a non-relativistic model, we adjusted the parameters and developed a physically realistic model by substituting the diskbb component with the kerrbb model (Li et al. 2005) to determine the black hole’s spin (Model 2: `tbabs*(kerrbb +powerlaw)`).

In the continuum-fitting method, parameters such as the black hole mass, source distance, and system inclination are crucial and significantly impact the results. But for the MAXI J1727-203, these parameters have not been precisely determined. Wang et al. (2022) constrained the black hole mass to be $11.5 M_{\odot} \leq M \leq 350.5 M_{\odot}$ for a distance of $5.9 \text{ kpc} \leq D \leq 57.3 \text{ kpc}$. Draghis et al. (2023b) obtained the inclination angle of this system to be 60^{+10}_{-7} degrees using the relativistic reflection method.

Due to the lack of precise measurements for these parameters, we at first systematically varied the distance, mass, and inclination within the relatively broad parameter ranges previously established in our study, using a step size of 0.1. Additionally, we attempted to fit the model by allowing all three parameters to vary, and found that similar results could be obtained within the same parameter ranges. Ultimately, the best fit is achieved with a black hole mass of approximately $12 M_{\odot}$, a distance of around 6 kpc, and an inclination angle of roughly 30° . The fitted results for the mass and distance fall within the parameter ranges reported in previous studies and are close to the lower limits of those ranges (Wang et al. 2022). So in subsequent fittings, we fix the black hole mass at $M_{\text{BH}} = 12 M_{\odot}$, the distance at $D = 6 \text{ kpc}$ and inclination angle at 30° , fitting the spin as free parameters. Based on the fitting results from the non-relativistic model, the equivalent hydrogen column density in `tbabs` was fixed to $0.35 \times 10^{22} \text{ cm}^{-2}$ after averaging. We also examined the impact of freeing this parameter on the fit results and found that it had a negligible effect on the final spin fitting, while the hardening factor was fixed at 1.7 (Shimura & Takahara 1995). We present the fitting results in Table 3, examples of the spectra and residuals in

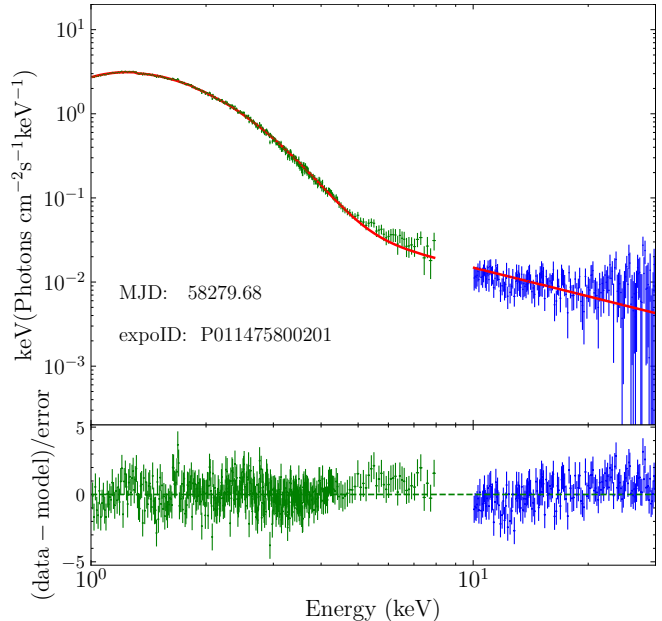


Figure 5. The spectrum and residuals for the relativistic model are shown as an example. The green and blue data points correspond to LE and ME, respectively. The observation time and expoID are labeled on the plot.

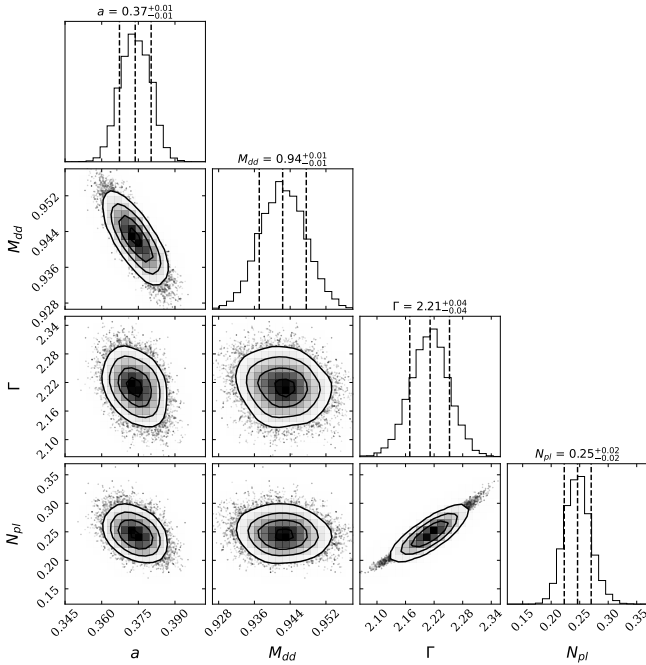
Fig 5, and the probability distribution of the parameters in Fig 6.

In addition, we also utilized the `tbabs*SIMPL*kerrbb` model to fit the observational data (e.g. ExpoID P011475800201) to examine whether different models would significantly affect the measurement of the spin parameter. SIMPL model (Steiner et al. 2009) represents the Comptonization of a seed spectrum, where a fraction of photons are scattered into a power-law distribution. The fitting results indicate that the impact of different non-thermal emission models on the spin parameter is minimal. Compared with `powerlaw` (Model 2), the spin value changes slightly from about 0.37 to 0.34, while the mass accretion rate increases from 0.94 to 1.001. Therefore, we only used Model 2 for subsequent analysis.

3.2.3. Error Analysis

Table 3. The Results of Spectral Fitting the Insight-HXMT Data for Relativistic Model

| Component | Parameter | ExpoID | ExpoID | ExpoID |
|-----------|------------------------------------|------------------------|------------------------|------------------------|
| | | P011475800201 | P011475800202 | P011475800301 |
| kerrbb | a_* | $0.37^{+0.02}_{-0.02}$ | $0.38^{+0.02}_{-0.03}$ | $0.41^{+0.02}_{-0.01}$ |
| | M_{dd} [10^{18} g s $^{-1}$] | $0.94^{+0.02}_{-0.01}$ | $0.94^{+0.03}_{-0.02}$ | $0.79^{+0.02}_{-0.02}$ |
| powerlaw | Γ | $2.2^{+0.1}_{-0.1}$ | $2.2^{+0.2}_{-0.2}$ | $2.6^{+0.07}_{-0.08}$ |
| | Norm | $0.25^{+0.08}_{-0.06}$ | $0.24^{+0.12}_{-0.09}$ | $0.81^{+0.13}_{-0.12}$ |
| | χ^2/dof | 0.76 | 0.79 | 0.79 |

**Figure 6.** The corner plot of the posterior probability distributions derived from the MCMC analysis for the parameters in the relativistic model.

When fitting the spin using the continuum-fitting method, parameters such as distance, inclination, and mass have a significant impact on the final fitting results (McClintock et al. 2015). In line with previous work, we apply the Monte Carlo (MC) method to conduct error analysis (Gou et al. 2010; Zhao et al. 2020; Wu et al. 2023; Guan et al. 2024).

Due to the lack of precise measurements for the distance, inclination, and mass of MAXI J1727-203, which are only roughly estimated, our fitting results indicate the best fit around $(D, i, M) \approx (6\text{kpc}, 30^\circ, 12M_\odot)$. Thus, we set over 3000 sets of parameters within the ranges of $D \sim (5.9\text{kpc}, 7\text{kpc})$, $i \sim (24^\circ, 35^\circ)$, and $M \sim (10M_\odot, 14M_\odot)$. We assume that these parameters are independent and follow a uniform distribution. These parameters were evenly distributed to investigate the influence of different factors. Subsequently, we em-

ployed a relativistic model to fit the energy spectra from the three exposures, enabling us to determine the distribution of the spin.

During the fitting process, we found that many parameters did not yield satisfactory results, and in several parameter spaces, the fitted spin values were retrograde (for a detailed discussion, see the Sections 4). The distribution of spin for each spectrum is displayed in Fig 7, and the combined histogram is presented in Fig 8. We used the generalized logistic distribution to fit the spin distribution we obtained. Its probability density function is:

$$f(x, c) = c \frac{\exp(-x)}{(1 + \exp(-x))^{c+1}}, \quad (1)$$

where c is the shape parameters. In Fig 7, we present the spin distribution obtained from the three observations and the fitted curves. The red solid line represents the fitted probability density distribution, while the position of the black dashed line corresponds to the peak of the probability density distribution. The red dashed line marks the position corresponding to 1σ . The corresponding ExpoIDs are labeled on the plot. Fig 8 shows the combined histogram and the corresponding fitted curve. The markings in the figure are consistent with those in In Fig 7. The final spin value we obtained is $a = 0.34^{+0.15}_{-0.19}$ (1σ).

4. DISCUSSION

4.1. Effect of Different Parameter Configurations

As we mentioned above, after traversing the entire parameter space, we obtained a good fit to the spectrum within a relatively narrow range. The variations in mass, distance, and inclination angle can affect the measurement of the black hole spin. For this source, these parameters have significant uncertainties; therefore, we need to examine the impact of different parameter values on the results of the spin measurement. In Fig 9, we present the relationship between the parameter and the spin over a broader range. From the figure, it can be observed that the spin value gradually increases as the black hole mass increases. However, as the inclination

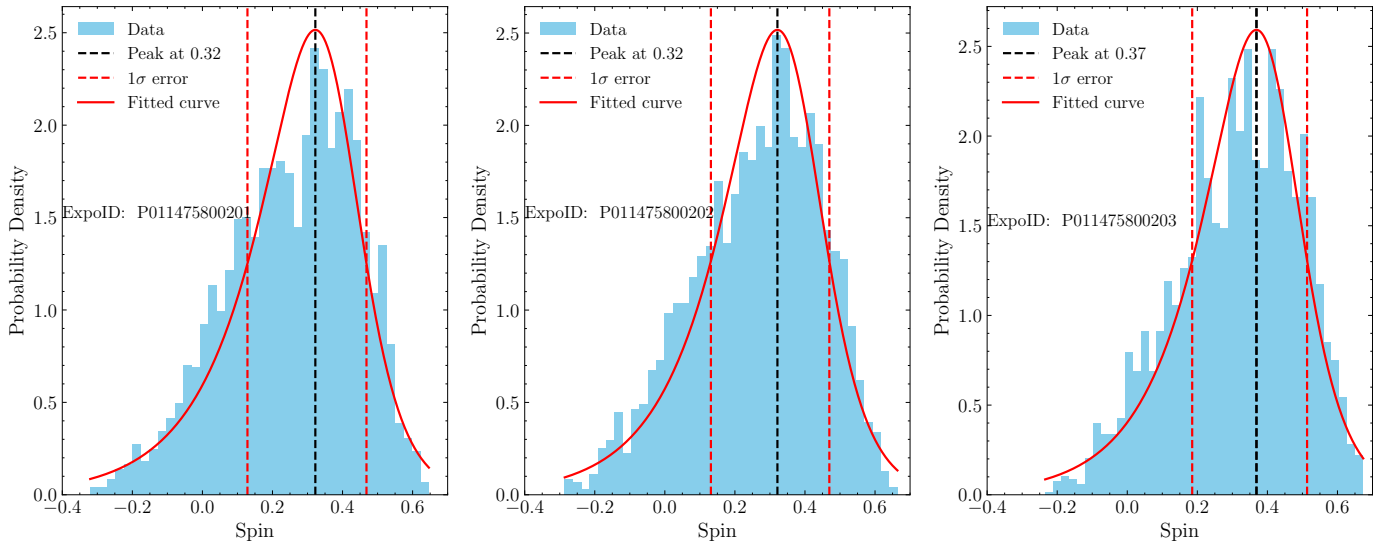


Figure 7. The distribution of a_* from the Monte Carlo method for the fitting results of the three exposures. The red dash lines represent the 1σ error, the black dashed lines indicate the best-fitting value, and the red line shows the generalized logistic distribution fitting. The corresponding expoID is labeled on the plot.

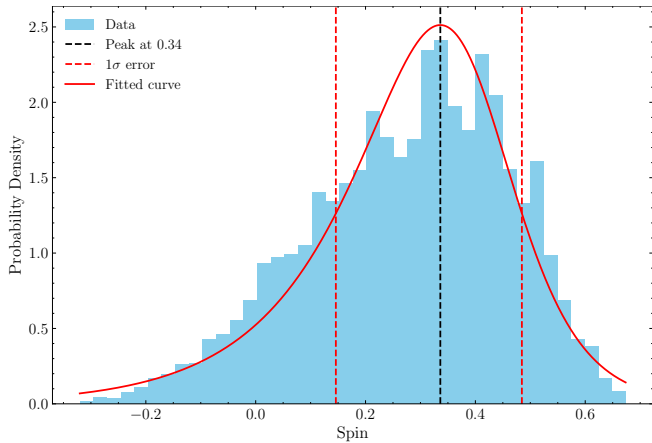


Figure 8. The summed distribution of a_* from the Monte Carlo method for the fitting results of the three exposures, with a total of 9000 data points. The red dash lines represent the 1σ error, the black dashed lines indicate the best-fitting value, and the red line shows the generalized logistic distribution fitting.

angle and distance increase, the spin decreases sharply, leading to a retrograde black hole.

Since most the black hole spins obtained using the continuum-fitting method are positive (Steiner et al. 2011, 2016; Chen et al. 2016; Zhao et al. 2021; Feng et al. 2023; Wu et al. 2023; Guan et al. 2024; Sai et al. 2024; Chen & Wang 2024), and there has been no clear observational evidence for the existence of retrograde black holes, this suggests that the results of a retrograde black hole must be interpreted with caution.

Morningstar et al. (2014) initially reported a retrograde spin for the black hole in Nova Muscae 1991, with a spin parameter of $a = -0.25^{+0.05}_{-0.64}$ (90% confi-

dence level). However, they noted that this measurement could be better constrained if the distance to the binary and the mass of the black hole were more accurately determined. Subsequently, with more accurate estimates of the black hole mass, the orbital inclination angle of the system and the distance, Chen et al. (2016) obtained a spin parameter of $a = 0.63^{+0.16}_{-0.19}$ (1σ).

In the study of MAXI J1659-152, Feng et al. (2022), based on the more accurate distance, mass, and inclination information provided by Torres et al. (2021) through spectroscopy, with $i = 70^\circ - 80^\circ$, $D = 6 \pm 2$ kpc, and $M = 4.9 - 5.7M_\odot$, investigated the spin of this source using the continuum-fitting method. They found that the spin parameter was constrained to $-1 < a \lesssim 0.44$ (90% confidence), with an inverse correlation to the inclination angle, then for the young age of this system, an extreme retrograde spin remains possible.

In the `kerrbb` model, a strong correlation exists between the accretion rate (or luminosity) and the spin parameter. As the spectral hardening factor can vary with luminosity (Davis et al. 2006), it is also inversely correlated with the spin parameter, as shown in Figure 4 of Salvesen & Miller (2021). Previously, we fixed the hardening factor at 1.7, so we also treat it as a free parameter to investigate its impact on the measured spin values. We chose the first observation as an example to perform the spectral fittings again, allowing the hardening factor to vary between 1.5 and 1.8, during which the spin parameter changed from about 0.65 to 0.2. Subsequently, we generated 100 evenly spaced values for the hardening factor in the range of 1.65 to 1.75 and performed fittings to derive the relationship between the

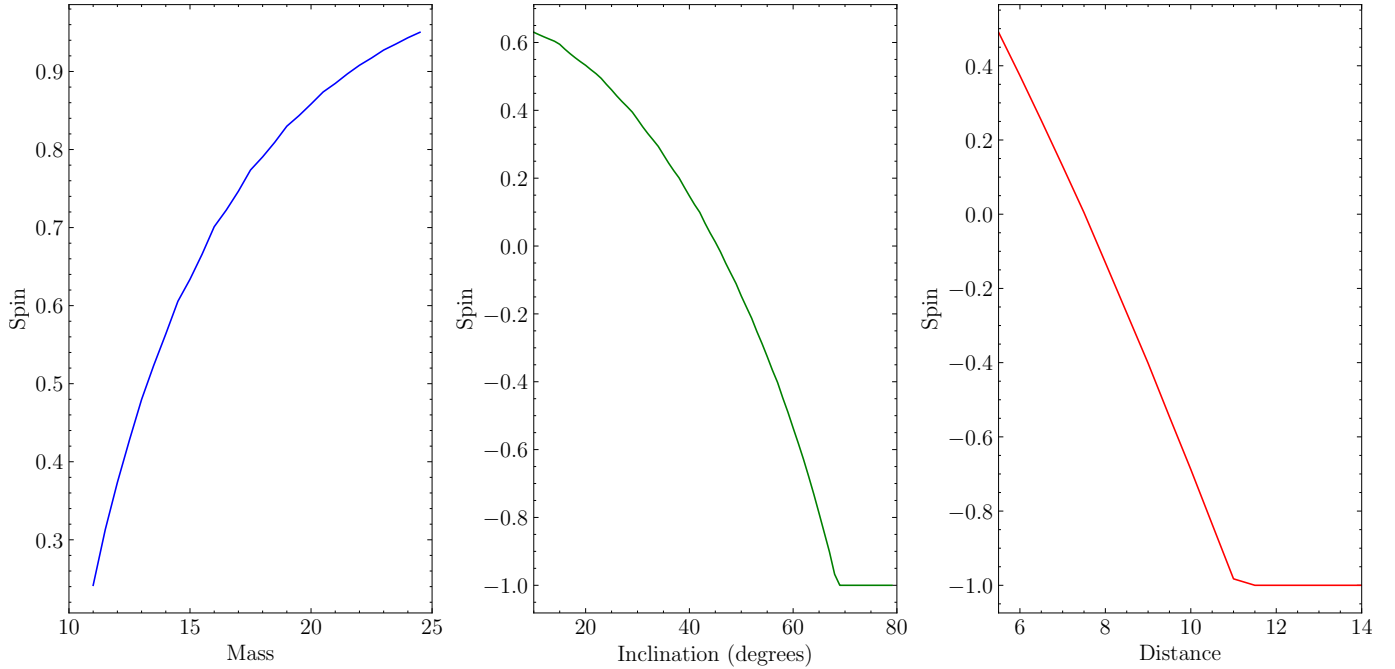


Figure 9. Correlation plots illustrating the impact of varying M , i , and D on measuring the spin.

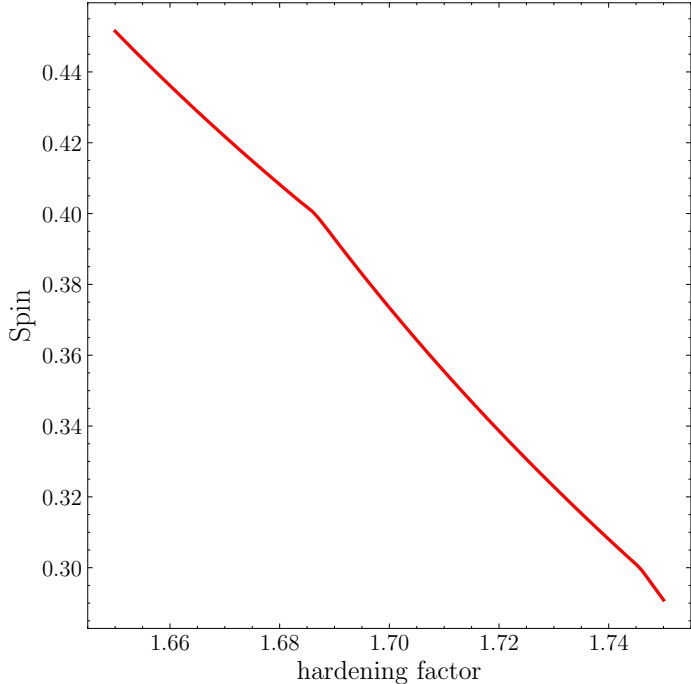


Figure 10. Correlation plots illustrating the impact of varying hardening factor on measuring the spin.

spin parameter and the hardening factor which is presented in Figure 10. It can be seen that there is an inverse correlation between the spin parameter and the hardening, consistent with previous studies (Salvesen & Miller 2021; Wu et al. 2023; Guan et al. 2024).

4.2. Re-fitting of NuSTAR spectra in LHS

Draghis et al. (2023a) applied the reflection method based on the *relxill* family of models to estimate the spin of MAXI J1727-203 using a NuSTAR observation taken during the phase when the source had just entered the LHS. However they found an extreme black hole spin of $0.986^{+0.012}_{-0.159}$ and a high inclination of 64^{+10}_{-7} degrees. The spin value obtained from the reflection fit is significantly higher than the result based on the continuum model in this work. To resolve the difference of the spin measurement for two methods, we also analyzed the NuSTAR spectra during the low hard state (LHS) to constrain the possible reflection components. Here, we focused on the NuSTAR observation of MAXI J1727-203 with ObsID 90401329002 as the example, a detailed description of the data processing procedure is also provided in the Appendix A.

We used the `tbabs*(diskbb+powerlaw)` model to fit the energy spectra of FPMA and FPMB. We allowed the hydrogen column density of *tbabs* to vary, resulting in $\chi^2/\nu = 1749.07/1772 = 0.987$. The fitting result for the hydrogen column density is $(3.948 \pm 0.466) \times 10^{22} \text{cm}^{-2}$, in the *diskbb* model, the inner disk temperature (T_{in}) is 0.500 ± 0.013 keV, and the normalization ($diskbb_{\text{norm}}$) is 516.209 ± 141.615 . In the *powerlaw* model, the photon index (Γ) is 1.77 ± 0.007 . We present the fitting results in Fig 11, we can observe that there are no significant reflection features in the residuals. Therefore, we believe that the previous studies, when fitting with the *tbabs* \times (*diskbb* + *powerlaw*) model, may have improperly fitted the parameters, leading to the appear-

ance of the iron line feature in the residuals (Draghis et al. 2023a). This likely caused the large discrepancy between the spin values obtained using the reflection model and those we derived. However, since the detailed fitting parameters of their results were not presented, we are unable to make a direct comparison. In addition, Negoro et al. (2018) found the disk component below 3 keV, while the energy range used in the NuSTAR data fitting is above 3 keV, which could also potentially cause iron line issues with the fitting results. Subsequently, we will conduct a detailed spectral analysis of the NICER observations of MAXI J1727-203 during its outburst, hoping to identify possible prominent reflection features.

It is worth noting that the spin values of the black holes in X-ray binaries obtained from fitting using the reflection method are generally larger than those derived from continuum-fitting (Reynolds 2021). In the spin measurement of MAXI J1348-630, Song et al. (2023) used the reflection model to fit the Insight-HXMT data and constrained the spin parameter to be $0.82^{+0.04}_{-0.03}$ (90 percent confidence). Draghis et al. (2024) measured the spin of MAXI J1348-630 based on relativistic reflection, obtaining a spin value of $0.977^{+0.017}_{-0.055}$ and an inclination angle of 52^{+8}_{-11} degrees. This result also shows a significant difference compared to the spin value of $0.78^{+0.04}_{-0.04}$ and inclination angle of $29.2^{+0.3}_{-0.5}$ degrees based on the reflection model using NuSTAR data reported by Jia et al. (2022). Jia et al. (2022) fixed the emissivity indices ($q_1 = q_2 = 3$), meaning their spin measurement represents a lower limit. They also did not account for narrow absorption features in the spectra. Draghis et al. (2024) results show higher spin values, as expected when allowing the emissivity parameters to vary freely. Additionally, the inclusion of Gaussian absorption features increases the inclination angle, leading to a higher measurement. Recently, Wu et al. (2023) obtained a spin of $0.42^{+0.13}_{-0.50}$ using the continuum-fitting method. Guan et al. (2024) estimated the spin of MAXI J1348-630 using the continuum-fitting method, obtaining a value of 0.79 ± 0.13 . They suggest that the accuracy of spectral fitting, particularly of the continuum spectrum, may affect the reflection component and spin measurements.

For the other black hole candidate 4U 1543-47, a similar situation also occurred. Yang et al. (2024) used observations from Insight-HXMT and employed the X-ray reflection fitting method to analyze the spectral data and measure the spin, and estimated the spin parameter of the black hole to be $0.902^{+0.054}_{-0.053}$ (90 percent confidence). Chen & Wang (2024) determined the spin of 4U 1543-47 using the thermal continuum-fitting method, which is sensitive to parameters such as black hole mass, distance, and inclination. Adopting their pre-

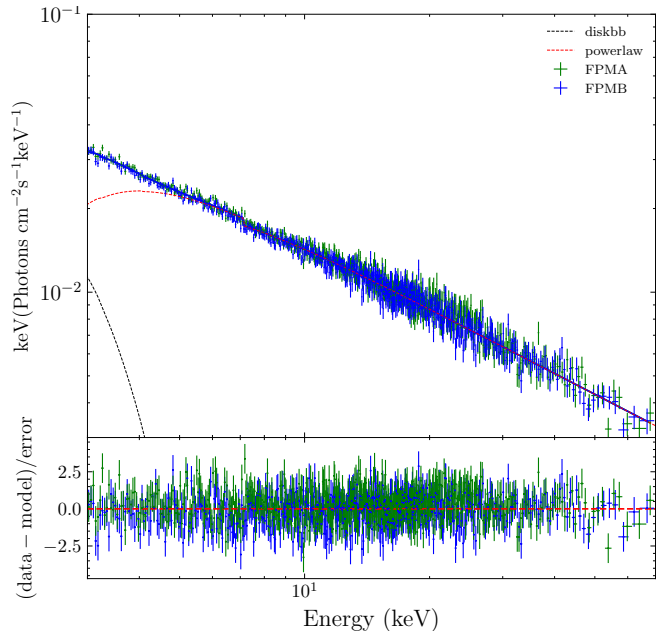


Figure 11. The top panel shows the spectrum of MAXI J1727-203, with the NuSTAR FPMA spectrum in green and the FPMB spectrum in blue. The reported best-fit model $\text{tbabs}*(\text{diskbb} + \text{powerlaw})$ is represented by the blue solid lines, while the contribution of the `diskbb` component is shown by the black dashed line. The red dashed line represents the `powerlaw` component. The bottom panel displays residuals. The red dashed line marks the position where the residuals are zero.

ferred values of $M = 9.4 \pm 1 M_{\odot}$, $D = 7.5 \pm 0.5$ kpc, and $i = 36.3^{+5.3}_{-3.4}$ degrees, they obtained a moderate spin of $a = 0.46 \pm 0.12$.

5. CONCLUSIONS

In this work, we present the BH spin results for MAXI J727-203 based on Insight-HXMT observations during the HSS using the continuum-fitting method. Since the spin of the black hole is highly sensitive to the measurements of the disk inclination, black hole mass, and distance for the binary system, the absence of dynamical measurements results leads to significant uncertainties in these parameters, making it challenging to accurately assess the spin. Based on previous rough estimates of these parameters, we explored the entire parameter space, and found that within the consistent value ranges, we achieved good fitting results around $(D, i, M) \approx (6 \text{ kpc}, 30^{\circ}, 12M_{\odot})$ using the relativistic model. Furthermore, due to the considerable uncertainty in the input parameters D , M , and i , we tested the influence of these parameters using Monte Carlo methods. Over 3000 sets of parameters were randomly sampled within the ranges $D \sim (5.9 \text{ kpc}, 7 \text{ kpc})$, $i \sim (24^{\circ}, 35^{\circ})$, and $M \sim (10M_{\odot}, 14M_{\odot})$ to fit the spectra. By combining

the spin distributions from these fits, we obtained a spin value of $a = 0.34_{-0.19}^{+0.15}$ (1σ). The hardening factor also affects the measurement of a in the continuum-fitting model, and there exists an anti-correlation between the spin parameter and hardening factor. Additionally, we processed the NuSTAR observations in the LHS. We found that using the `tbabs*(diskbb +powerlaw)` model provided a good fit, with no significant iron line features observed in the residuals. We believe this is the reason for the discrepancy between the high spin values obtained from previous reflection model fits and our continuum-fitting results.

ACKNOWLEDGEMENTS

We are grateful to the referee for the suggestions to improve the manuscript. This work is supported by the National Key Research and Development Program of China (Grants No. 2021YFA0718503 and 2023YFA1607901), the NSFC (12133007), the Youth Program of Natural Science Foundation of Hubei Province (2024AFB386) and the Postdoctoral Fellowship Program (Grade C) of China Postdoctoral Science Foundation (Grant No. GZC20241282). This work has made use of data from the *Insight*-HXMT mission, a project funded by the China National Space Administration (CNSA) and the Chinese Academy of Sciences (CAS).

REFERENCES

- Alabarta, K., Altamirano, D., Méndez, M., et al. 2020, *Monthly Notices of the Royal Astronomical Society*, 497, 3896
- Bardeen, J. M., Press, W. H., & Teukolsky, S. A. 1972, *Astrophysical Journal*, Vol. 178, pp. 347-370 (1972), 178, 347
- Belloni, T. M. 2010, in *The Jet Paradigm: From Microquasars to Quasars* (Springer), 53–84
- Cao, X., Jiang, W., Meng, B., et al. 2020, *Science China Physics, Mechanics & Astronomy*, 63, 1
- Chen, J., & Wang, W. 2024, *Monthly Notices of the Royal Astronomical Society*, 527, 238
- Chen, Y., Cui, W., Li, W., et al. 2020, *Science China Physics, Mechanics & Astronomy*, 63, 1
- Chen, Z., Gou, L., McClintock, J. E., et al. 2016, *The Astrophysical Journal*, 825, 45
- Davis, S. W., Done, C., & Blaes, O. M. 2006, *The Astrophysical Journal*, 647, 525
- Draghis, P. A., Miller, J. M., Costantini, E., et al. 2024, *The Astrophysical Journal*, 969, 40
- Draghis, P. A., Miller, J. M., Zoghbi, A., et al. 2023a, *The Astrophysical Journal*, 946, 19
- Draghis, P. A., Miller, J. M., Homan, J., et al. 2023b, *The Astronomer’s Telegram*, 16219, 1
- Fabian, A., Rees, M., Stella, L., & White, N. E. 1989, *Monthly Notices of the Royal Astronomical Society*, 238, 729
- Fender, R., & Belloni, T. 2004, *Annu. Rev. Astron. Astrophys.*, 42, 317
- Feng, Y., Steiner, J. F., Ramirez, S. U., & Gou, L. 2023, *Monthly Notices of the Royal Astronomical Society*, 520, 5803
- Feng, Y., Zhao, X., Li, Y., et al. 2022, *Monthly Notices of the Royal Astronomical Society*, 516, 2074
- Gendreau, K. C., Arzoumanian, Z., Adkins, P. W., et al. 2016, in *Space telescopes and instrumentation 2016: Ultraviolet to gamma ray*, Vol. 9905, SPIE, 420–435
- Gou, L., McClintock, J. E., Steiner, J. F., et al. 2010, *The Astrophysical Journal Letters*, 718, L122
- Guan, J., Ma, R., Tao, L., et al. 2024, *The Astrophysical Journal*, 976, 61
- Jia, N., Zhao, X., Gou, L., et al. 2022, *Monthly Notices of the Royal Astronomical Society*, 511, 3125
- Kennea, J., Bahramian, A., & Beardmore, A. 2018, *The Astronomer’s Telegram*, 11697, 1
- Kerr, R. P. 1963, *Physical review letters*, 11, 237
- Kulkarni, A. K., Penna, R. F., Shcherbakov, R. V., et al. 2011, *Monthly Notices of the Royal Astronomical Society*, 414, 1183
- Li, L.-X., Zimmerman, E. R., Narayan, R., & McClintock, J. E. 2005, *The Astrophysical Journal Supplement Series*, 157, 335
- Liu, C., Zhang, Y., Li, X., et al. 2020, *Science China Physics, Mechanics & Astronomy*, 63, 1
- Ludlam, R., Bult, P., Gendreau, K., et al. 2018, *The Astronomer’s Telegram*, 11689, 1
- McClintock, J. E., Narayan, R., & Steiner, J. F. 2015, *The Physics of Accretion onto Black Holes*, 295
- Morningstar, W. R., Miller, J. M., Reis, R. C., & Ebisawa, K. 2014, *The Astrophysical Journal Letters*, 784, L18
- Negoro, H., Shidatsu, M., Mihara, T., et al. 2018, *The Astronomer’s Telegram*, 11696, 1
- Noble, S. C., Krolik, J. H., & Hawley, J. F. 2009, *The Astrophysical Journal*, 692, 411
- Novikov, I., Thorne, K., Dewitt, C., & Dewitt, B. 1973
- Penna, R. F., McKinney, J. C., Narayan, R., et al. 2010, *Monthly Notices of the Royal Astronomical Society*, 408, 752

- Remillard, R. A., & McClintock, J. E. 2006, *Annu. Rev. Astron. Astrophys.*, 44, 49
- Reynolds, C. S. 2021, *Annual Review of Astronomy and Astrophysics*, 59, 117
- Reynolds, C. S., & Fabian, A. C. 2008, *The Astrophysical Journal*, 675, 1048
- Reynolds, C. S., & Nowak, M. A. 2003, *Physics Reports*, 377, 389
- Sai, N., Wang, W., & Wu, H. 2024, *Journal of High Energy Astrophysics*, 43, 44
- Salvesen, G., & Miller, J. M. 2021, *Monthly Notices of the Royal Astronomical Society*, 500, 3640
- Shimura, T., & Takahara, F. 1995, *Astrophysical Journal*, Part 1 (ISSN 0004-637X), vol. 445, no. 2, p. 780-788, 445, 780
- Song, Y., Jia, N., Yang, J., et al. 2023, *Monthly Notices of the Royal Astronomical Society*, 526, 6041
- Steiner, J. F., Narayan, R., McClintock, J. E., & Ebisawa, K. 2009, *Publications of the Astronomical Society of the Pacific*, 121, 1279
- Steiner, J. F., Walton, D. J., García, J. A., et al. 2016, *The Astrophysical Journal*, 817, 154
- Steiner, J. F., Reis, R. C., McClintock, J. E., et al. 2011, *Monthly Notices of the Royal Astronomical Society*, 416, 941
- Tomsick, J., Shaw, A., Garcia, J., et al. 2018, *The Astronomer's Telegram*, 11881, 1
- Torres, M., Jonker, P., Casares, J., Miller-Jones, J., & Steeghs, D. 2021, *Monthly Notices of the Royal Astronomical Society*, 501, 2174
- Wang, S., Kawai, N., Shidatsu, M., et al. 2022, *Monthly Notices of the Royal Astronomical Society*, 514, 5320
- Wilms, J., Allen, A., & McCray, R. 2000, *The Astrophysical Journal*, 542, 914
- Wu, H., Wang, W., Sai, N., Zhu, H., & Chen, J. 2023, *Monthly Notices of the Royal Astronomical Society*, 522, 4323
- Yang, J., Jia, N., Qiao, E., Song, Y., & Gou, L. 2024, *Monthly Notices of the Royal Astronomical Society*, 532, 1410
- Yoneyama, T., Negoro, H., Nakajima, M., et al. 2018, *The Astronomer's Telegram*, 11683, 1
- Zhang, S. N., Cui, W., & Chen, W. 1997, *The Astrophysical Journal*, 482, L155
- Zhao, X., Gou, L., Dong, Y., et al. 2021, *The Astrophysical Journal*, 916, 108
- Zhao, X.-S., Dong, Y.-T., Gou, L.-J., et al. 2020, *Journal of High Energy Astrophysics*, 27, 53

APPENDIX

A. NUSTAR OBSERVATION

MAXI J1727-203 was observed by NuSTAR on July 26, 2018 (ObsID: 90401329002). In accordance with standard procedures³, we processed the NuSTAR data using HEASoft v6.32 with calibration files v20230816. To extract the source spectra, we used a circular region centered on the source position with a radius of 120", and background spectra were extracted using the same radius. Standard data processing tools were employed to generate level 2 (*nupipeline*) and level 3 (*nuproducts*) products. All spectra were grouped to ensure a minimum of 25 counts per energy bin, and χ^2 statistics were applied.

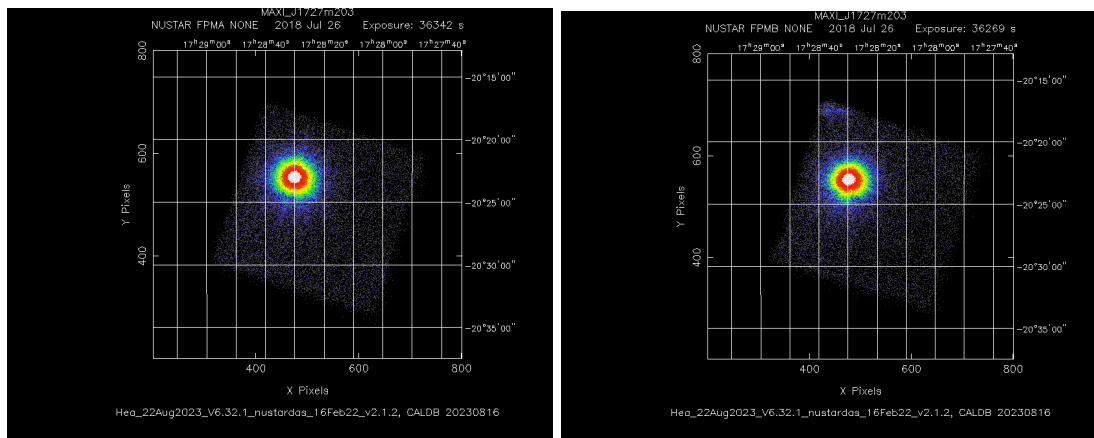


Figure A1. The position of MAXI J1727-203 in the NuSTAR field of view is shown. The left panel displays the FPMA, while the right panel shows the FPMB. The software version and CALDB version used for data processing are indicated on the plot.

³ <https://heasarc.gsfc.nasa.gov/docs/nustar/analysis/>